The Photogrammetric Record 23(124): 353–371 (December 2008)

DMC GEOMETRY ANALYSIS AND VIRTUAL IMAGE CHARACTERISATION

RAMON ALAMÚS (ramon.alamus@icc.cat)
WOLFGANG KORNUS (wolfgang.kornus@icc.cat)
Institut Cartogràfic de Catalunya, Barcelona, Spain

(Extended version of a paper submitted to the ISPRS Hannover Workshop on "High-resolution earth imaging for geospatial information" held at Leibniz Universität Hannover, Germany, 29th May to 1st June 2007)

Abstract

Since the advent of the first large format digital aerial cameras, high expectations have been placed on their performance. The dream of obtaining aerial images virtually free of geometric errors and with greater radiometric quality is getting close. Nevertheless, systematic image residuals, unexpected height errors in aerial triangulation and the need for additional self-calibration parameters have been reported since 2005. In this paper a preliminary analysis of the theoretical accuracies in aerial triangulation using the Zeiss/Intergraph (Z/I) Digital Mapping Camera (DMC) and an analogue camera is conducted, motivated by those recent reports. This analysis considers a mathematical model where the image has conical geometry and is free of systematic errors. The influence on the propagated block accuracy of the base-to-height ratio, image pointing precision (both manual and automatic), GPS observations for projection centres and of pass/tie point density is studied. Moreover, the expected accuracy in the aerial triangulation of analogue images using current procedures (having regard to the a priori accuracy for image pointing, ground control measurement and GPS and pass/tie point density) is computed. The goal of this theoretical study is to find the requirements for aerial triangulation with DMC data which would yield the same or an even higher level of accuracy than that obtained with analogue data under the same conditions.

The paper continues with a check on the conclusions of this theoretical analysis, using real data-sets and aerial triangulation set-up, which fit with the theoretical analysis. The results prove that the expected theoretical accuracy in aerial triangulation is only obtained if an appropriate self-calibration parameter set is considered in the bundle block adjustment and/or if good GPS observations are available. These requirements result from the unfavourable propagation from unmodelled systematic error in the DMC image blocks. Some authors have detected systematic residuals in the order of one-tenth of a pixel rms in DMC image space. For this reason, investigations are being carried out on systematic error characterisation, distribution in image space and stability over time and flying height, and systematic error modelling, using self-calibration parameter sets and applying correction grids. Finally, conclusions are drawn from the investigations.

KEYWORDS: accuracy, digital aerial camera, geometric calibration

INTRODUCTION

IN 2004 AND 2005 the Institut Cartogràfic de Catalunya (ICC) acquired two digital Zeiss/Intergraph (Z/I) Digital Mapping Cameras (DMC). Since the beginning, despite the good radiometric and geometric performance of the cameras, height accuracy at check points has not always been as good as expected. In fact, some authors (Alamús et al., 2006; Schroth, 2007) have reported unexpected large height errors.

Motivated by those results, this paper firstly compares the theoretical accuracy expected from photogrammetric point determination with the DMC to the accuracy achieved with analogue cameras, under similar set-up conditions to the data-sets in the papers under reference. Secondly, it demonstrates that, in fact, at least under certain conditions, height accuracy is worse than expected, but that this can be compensated to a large extent by using a suitable self-calibration approach. Thirdly, it states how such loss of accuracy is related to systematic errors in image space. Those systematic errors are calibrated/characterised and their stability in relation to time and flying height is discussed. The paper studies the capability of self-calibration parameters and calibration grids to compensate for systematic errors in image space.

DMC DESCRIPTION

The DMC simultaneously captures one high-resolution panchromatic image of $13\,824 \times 7680$ pixels (across-track and along-track, respectively) and four multispectral images (red, green, blue and near-infrared) of 3072×2048 pixels. The high-resolution image is formed from four images acquired with four inclined high-resolution panchromatic camera heads each with a focal length of 120 mm. Each of these camera heads covers a quarter of the final image, described as the virtual high-resolution image. Each low-resolution multispectral image in the red, green, blue and near-infrared colour bands is acquired with four additional nadir-looking camera heads with a focal length of 25 mm. These four images completely cover the virtual image (see Hinz, 1999; Zeitler et al., 2002; Dörstel et al., 2003 for details).

ON THEORETICAL ACCURACY

As there are some recent reports (Alamús et al., 2005, 2006; Schroth, 2007) on larger errors in bundle block adjustment than theoretically expected with DMC images, in this section the theoretical height accuracy in object space is analysed using simulations. The focus is on error propagation through the block rather than on height accuracy in a single model. Thus, the influence of the following four parameters is investigated: (1) base-to-height (B/H) ratio, (2) image observation accuracy, (3) GPS observation accuracy and (4) image point density. The main goal of this study is to find the requirements for aerial triangulation (aerotriangulation for convenience throughout the remainder of this paper) with DMC images, which would yield the same or even a higher level of accuracy than that obtained with analogue cameras under the same conditions.

The simulations consider the characteristics of the two cameras described in Table I representing a standard analogue camera and the DMC with a B/H ratio of 0·31. In order to simplify the analysis of theoretical accuracy, a single image strip of 5 km length with four ground control points (GCPs) at the four corners is used. A conventional von Gruber point

TABLE I. Features of the cameras used in the simulations (pixel size represents scanning size for the analogue camera).

Camera	*Focal length (mm)*	*Pixel size (μm)*	*Number of pixels columns × rows*	*B/H*
Analogue	150	15	15 000 × 15 000	0·60
DMC	120	12	7680 × 13 824	0·31

distribution scheme of three pass points is assumed, resulting in three rows of points, located at the edges and in the centre of the strip. The flying height is 1000 m (which is the altitude of the data-sets used in the referenced papers which reported unexpected large errors), the ground sampling distance (GSD) is 10 cm and the forward overlap is 60% in all simulations.

Influence of the Base-to-Height Ratio

This subsection discusses the influence of the base-to-height ratio on theoretical height accuracy. In general, the *B/H* ratio of large-format frame-based aerial digital cameras is reduced due to design or construction restrictions. The standard value of 0·60 with analogue aerial cameras is reduced to 0·31 in the case of the DMC. To compensate for this reduction by a factor of 2 of the *B/H* ratio, weighting values for image observations for DMC are set to approximately double the weight that is currently standard for analogue cameras at ICC. Such weighting is sensible provided that DMC image quality is good enough. Thus, weighting is set to 2 μm for the DMC and to 5 μm for the analogue camera. GCP weighting is set to 4 cm in planimetry and to 6 cm in altimetry. No GPS observations are included in the simulations.

In Fig. 1, the standard deviations in height for the pass points located in the centre of the strip are plotted. Two major effects are observed:

(a) Height accuracy degrades with reducing *B/H* and is worse for the DMC, as expected.
(b) The deterioration of height accuracy due to the low *B/H* of the DMC is not compensated for by the image observation accuracy only, which is twice as high (2 μm corresponds to one-sixth of a pixel) as that of the analogue camera (5 μm corresponds to ⅓ pixel).

Although it is clear from equation (1) that, in a model, the reduction of the *B/H* ratio by a factor of 2 is compensated for by improving image pointing accuracy by a factor of 2, the assessment (b) does not contradict the theory because equation (1) is related to height accuracy within a single model while the analysis carried out in this section is related to error propagation through the block in aerotriangulation. Fig. 1 shows that, in the neighbourhood of

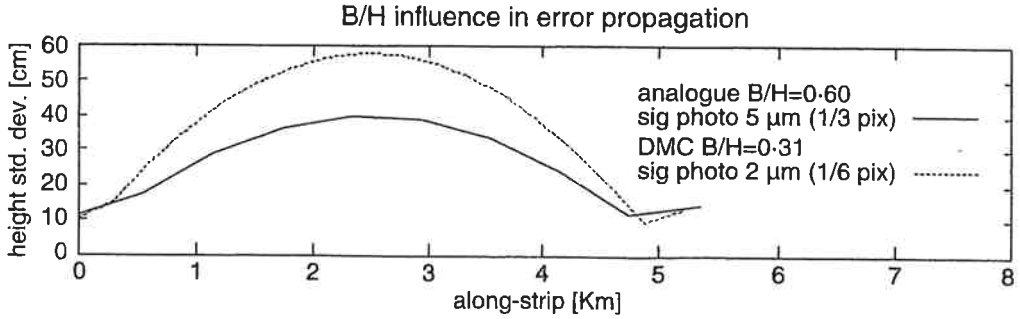

FIG. 1. Influence of the *B/H* ratio on theoretical height accuracies of pass points located at the strip centre.

a GCP at km 0, both analogue and DMC simulations have height accuracies consistent with the following equation:

$$\sigma_H = \sqrt{2}\frac{H^2}{Bf}\sigma_i \tag{1}$$

where: f = focal length;
H = flying height;
B = base length;
σ_i = image space accuracy; and
σ_H = height accuracy.

In summary, height accuracy deterioration caused by a halving of the B/H ratio cannot completely be compensated for by the double image pointing accuracy.

Influence of Image Observation Accuracy

In this subsection, the influence of image observation accuracy on the theoretically achievable height accuracy is analysed. Again, weighting values for image observations are set to 5 μm (ground control and pass/tie points) for the analogue camera. As the GCPs are supposed to be measured manually in a stereo workstation, for the DMC a weighting value of ⅓ pixel is used, corresponding to 4 μm. For pass/tie point observations weight values of 1·2, 1·5 and 2 μm are used. Where 1·2 μm corresponds to the expected 1/10 of a pixel accuracy using automatic matching techniques, 1·5 μm corresponds to the observed usual rms for image observation residuals according ICC experience (usually in the range from 1·5 to 1·8 μm) and 2 μm is the weight that compensates for the B/H reduction as explained in the section above. GCP weighting is set to 4 cm in planimetry and to 6 cm in altimetry. No GPS observations are included in the simulations.

The results in Fig. 2 suggest that DMC image observation accuracy must be in the range of 1·2 and 1·5 μm in order to achieve a comparable height accuracy in the simulation set-up, which would be obtained with a 5 μm observation accuracy in analogue images. According to the authors' experience, semi-manual pass point measurements can reach an image pointing accuracy of the order of 0·2 pixel (2·4 μm) and an automatic point matching accuracy of the order of 0·1 pixel (1·2 μm) (Alamús et al., 2005).

It should be kept in mind that error propagation depends on image pointing accuracy, GCP accuracy (as initial adjustment conditions) and the number of images between GCPs. In other words, with no GPS observations, the distance between GCPs must be adapted to the given

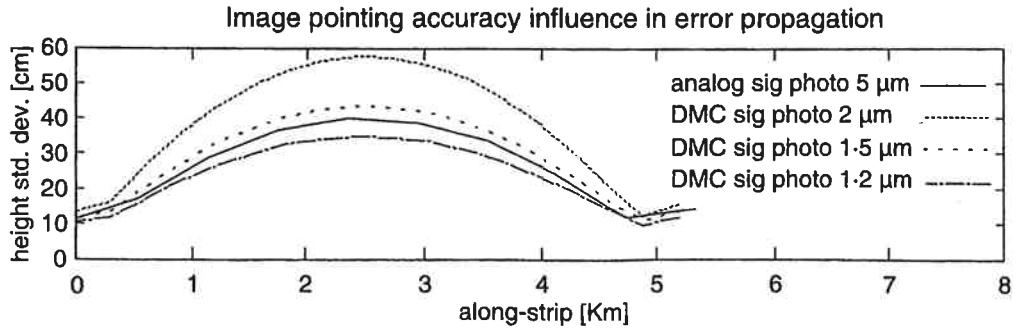

FIG. 2. Influence of image observation accuracy on theoretical height accuracies of pass points located at the strip centre.

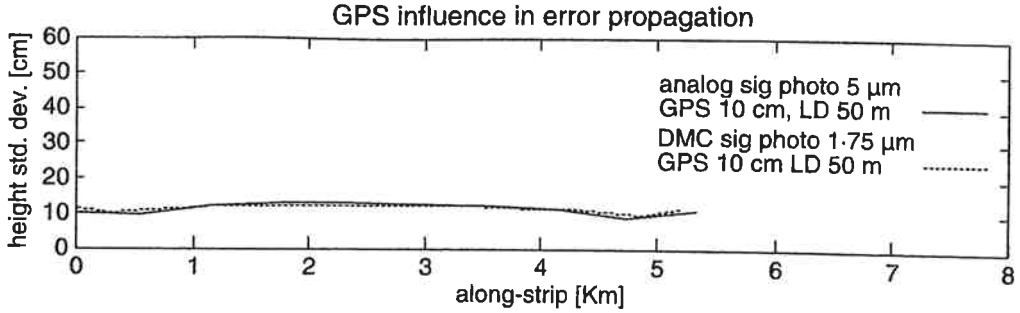

FIG. 3. Influence of GPS observations on theoretical height accuracies of pass points located at the strip centre.

image pointing accuracy to keep DMC height accuracy (due to error propagation) comparable to that of the analogue camera.

Influence of GPS Observations

This subsection is devoted to the influence of GPS observations on theoretical height accuracy. Again, weighting values are set to 5 µm for image observations (ground control and pass/tie points) for scanned analogue imagery. As GCPs are supposed to be measured manually in a stereo workstation, ⅓ pixel is assumed as a weight value that corresponds to 4 µm for the DMC. For pass/tie point observations a value of 1·75 µm is used, which corresponds to the observed usual rms for image observation residuals according ICC experience (usually in the range from 1·5 to 1·8 µm). GCP weighting is set to 4 cm in planimetry and to 6 cm in altimetry. Weighting for GPS observations is set to 10 cm and a linear drift parameter set, which is introduced with low weight (50 m), is considered.

Fig. 3 shows that the difference in the height accuracies caused by the different *B/H* values disappears if GPS observations are available. GPS weight settings of 10 cm lead to the same level of theoretical height accuracy for both the DMC and the analogue camera in the simulation set-up.

Influence of Image Point Density

This subsection focuses on the influence of a highly dense photogrammetric network (which, in practice, can be obtained by automatic aerotriangulation (AAT) procedures) on theoretical height accuracy. In these simulations a dense distribution of 80 points per image in the von Gruber positions is considered. Weighting values for image observations are set to 5 µm (ground control and pass/tie points) for the analogue camera. For the DMC, values are set to 4 µm for GCP observations and 1·75 µm for pass/tie point observations as explained above. GCP weighting is set to 4 cm in planimetry and 6 cm in altimetry. No GPS observations are included in the simulations.

The results in Fig. 4 show that a dense photogrammetric network also contributes to compensating for the lower height accuracy caused by the smaller *B/H* of the DMC. Thus, height accuracies are comparable to those obtained using GPS observations (see Fig. 3). In other words, in this simulation set-up AAT techniques lead to the same level of theoretical accuracy for both DMC and the analogue camera as does the inclusion of GPS observations in the bundle adjustment.

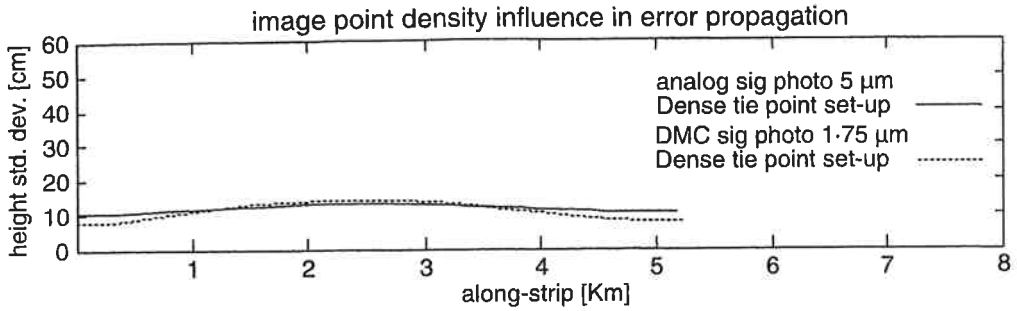

FIG. 4. Influence of image point density on theoretical height accuracies of pass points located at the strip centre.

ON PRACTICAL EXPERIENCE WITH THE DMC

Some authors (Alamús et al., 2005, 2006; Schroth, 2007) have reported that DMC block aerotriangulation generates larger height errors than were predicted by Dörstel (2003). Recent studies relate these height errors to systematic errors in DMC image space (Alamús et al., 2006; Honkavaara et al., 2006a, 2006b). The need for additional parameters which compensate for these unmodelled systematic errors in image space is currently being discussed in the community (Alamús et al., 2006; Cramer, 2007; Schroth, 2007). Results on the capability of using four sets of 12 self-calibration parameters to overcome unexpected large height errors are discussed here, and systematic errors in image space are analysed. Finally, stability and dependency on time and flying height of systematic errors in virtual image space are studied. For this analysis five real blocks at different image scales are used.

Data-sets

This section provides an overview of the different data-sets and a summary of the main features of the blocks used in the study (see Table II).

Block "Rubí". The Rubí data was acquired on 8th March 2005 with the DMC01-0014 camera. The block consisted of 426 images distributed in 13 parallel and three transverse strips taken at a flight altitude of 1000 m above ground level, which corresponds to a GSD of 10 cm. Nineteen natural GCPs and 426 orientations derived from airborne GPS/INS data were used to triangulate the block. Moreover, 20 well-distributed check points were measured in the images,

TABLE II. Data-set configuration.

Block	*Rubí*	*330*	*362*	*470*	*Castell*
GSD (m)	0·10	0·45	0·45	0·45	0·08
Flying height (m)	1000	4500	4500	4500	750
Forward overlap (%)	75	60	60	60	60
Lateral overlap (%)	50	30	30	30	30
Number of strips	16	4	4	4	4
Number of GPS/INS obs.	426	300	346	380	62
Number of images	426	300	346	380	62
Number of check points	20	9	7	8	None
Number of GCPs	19	40	32	43	16
Camera	DMC01-0014	DMC01-0026	DMC01-0026	DMC01-0026	DMC01-0026
Focal length (mm)	120	120	120	120	120

which belong to the fourth-order geodetic network of Rubí and have an accuracy of 2 cm in planimetry and 4 cm in altimetry.

Block 330. Block 330 was acquired on 27th and 28th May 2006 with the DMC01-0026 camera and covered a rectangular area of 88 km × 21 km, corresponding to three 1:50 000 map sheets. The block consisted of 300 images distributed in four parallel strips taken at an average altitude of 4500 m above ground level, which corresponds to a GSD of 0·45 m. The block contained 40 full natural GCPs, 9 natural check points and 300 orientations derived from airborne GPS/INS data.

Block 362. Block 362 was acquired mainly on 27th and 28th May and a few images on 5th June 2006 with the DMC01-0026 camera and covered a rectangular area of 88 km × 21 km, corresponding to three 1:50 000 map sheets. The block consisted of 346 images distributed in four parallel strips taken at an average altitude of 4500 m above ground level, which corresponds to a GSD of 0·45 m. The block contained 32 full natural GCPs, 7 natural check points and 346 orientations derived from airborne GPS/INS data.

Block 470. Block 470 was acquired on 1st and 21st June 2006 with the DMC01-0026 camera and covered a rectangular area of 90 km × 22 km, corresponding to three 1:50 000 map sheets. The block consisted of 380 images distributed in four parallel strips taken at an average altitude of 4500 m above ground level, which corresponds to a GSD of 0·45 m. The block contained 43 full natural GCPs, 8 natural check points and 380 orientations derived from airborne GPS/INS data.

Block "Castell". The Castell data was acquired on 7th May 2006 with the DMC01-0026 camera. The block consisted of 62 images distributed in two parallel and two transverse strips, which were parallel and with 30% side overlap, taken at a flight altitude of 750 m above ground level, which corresponds to a GSD of 7·5 cm. Sixteen natural GCPs and 62 orientations derived from airborne GPS/INS data were used to triangulate the block.

DMC Accuracy

In this section the achievable accuracy in aerotriangulation of the DMC is analysed using the Rubí data-set. The block adjustment is comparable to the set-up described in the above theoretical study, with the same weighting of GPS and image observations and a dense photogrammetric network obtained by automatic image matching techniques.

The number of object points, image observations and the DMC post-processing software (PPS) version were varied (see Table III) in four different aerotriangulation runs (AT 1 to AT 4) using the same ground control and check point observations. Images used in AT 1 were processed with DMC PPS version 4·4. Images used in AT 2, AT 3 and AT 4 were processed with DMC PPS version 5·1. Since the upgrade from version 4·4 to 5·1 implies a difference in geometry, it was not possible to use the same observations as in AT 1. The geometry of version

TABLE III. Number of image observations, corresponding number of object points and DMC PPS version for the four different aerotriangulations performed in block Rubí.

Aerotriangulation	*Number of image observations*	*Number of object points*	*DMC PPS version*
AT 1	45 462	7762	4·4
AT 2	25 959	4152	5·1
AT 3	32 858	4683	5·1
AT 4	187 810	34 695	5·1

5·0 and older is related to mid-exposure time while the geometry of version 5·1 is related to initial exposure time. This upgrade improves GPS time synchronisation, because the GPS time tag synchronisation pulse is generated at the initial exposure time instead of the mid-exposure time, but causes a shift in the image (between version 5·1 and older) corresponding to half the size of forward motion compensation (Hefele and Dörstel, 2007).

AT 1 and AT 2 are comparable in terms of block connection. Although AT 2 has a smaller number of image observations and corresponding object points than AT 1, they are better distributed and the average number of images connected by an object point is higher in AT 2 than in AT 1. For this reason, AT 2 compensates for the smaller number of points with better connected tie points leading to comparable block connection in both ATs.

The bundle block adjustments were computed using 10 cm a priori GPS accuracy and 2 μm a priori image pointing accuracy. According to the results of the simulation study discussed earlier, the use of this weighting configuration should yield similar results to current analogue data-sets. The four aerotriangulations were each calculated twice: without any additional parameter set and with one set of 12 self-calibration parameters per image quarter (four sets of 12 parameters in total) (see Alamús et al., 2006). Fig. 5 summarises the height accuracies obtained at the 20 check points. Three conclusions can be drawn from the results:

(1) The results obtained without additional parameters (in the background) become worse as the block connection becomes better (which is usually, but not necessarily, related to a larger number of image observations and corresponding object points). Similar effects are also described by Schroth (2007), who reports significantly larger height residuals at check points in a block with an 80% sidelap than in the same block with 60% sidelap or less.
(2) The results obtained with four sets of 12 self-calibration parameter computations show the same level of height accuracy almost independently of block redundancy.
(3) The results obtained for AT 1 and AT 2 are comparable in both computations (with and without additional parameters), which indicates that image geometry changes due to version upgrading do not affect the adjustment results significantly.

Fig. 6 illustrates the combined effect of varying GPS and image observation weights without using self-calibration. Height accuracy at the check points increases with decreasing

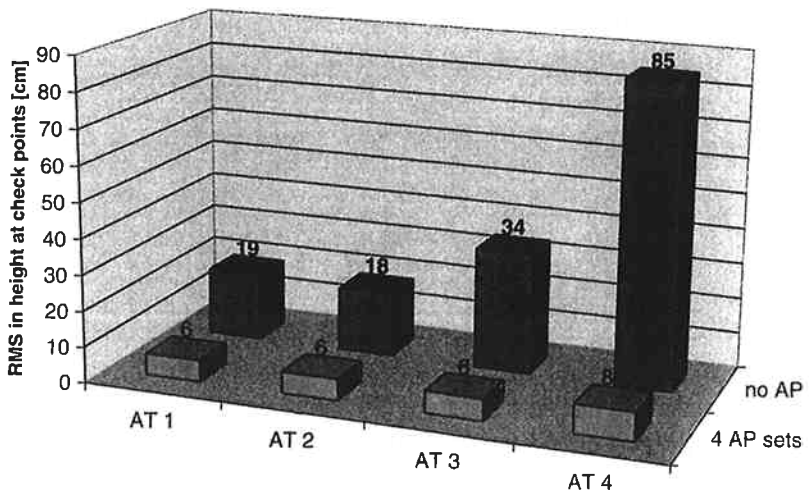

FIG. 5. Height accuracy dependency on redundancy and number of observations with and without additional parameters.

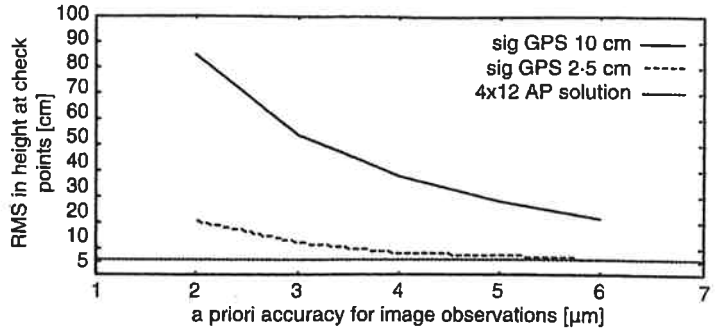

FIG. 6. Height accuracy dependency on GPS and image weighting. Block adjustments were performed without any additional self-calibration parameter set and using AT 4 (see Table III).

image observation weights. Highly weighted GPS observations ($\sigma = 2{\cdot}5$ cm) and low weighted image observations ($\sigma = 6$ μm) lead to similar good results as those achieved with low weighted GPS observations ($\sigma = 10{\cdot}0$ cm), highly weighted image observations ($\sigma = 2$ μm) and four sets of 12 additional self-calibration parameters. In this case, the block geometry is fixed by the GPS, and the image observations will obtain higher residuals which are otherwise absorbed by self-calibration.

Since the block adjustment set-up corresponds to the earlier simulation study (GPS weighting, image observation weighting and a large number of automatically derived pass/tie points), the results obtained should reveal height accuracies comparable to those reached with analogue data-sets, which is not the case. However, it is possible to overcome the unexpected large height errors (shown in Figs. 5 and 6 when no self-calibration is considered) by using an appropriate set of additional parameters in bundle block adjustment, which is a clear indication that image observations are influenced by systematic errors. The next subsection is therefore dedicated to the analysis of systematic errors in image space.

Systematic Errors in Image Space

Two topics are studied here: (a) characterisation of the systematic errors with the Rubí data-set, where their magnitude and distribution in image space are discussed, and (b) stability depending on flying height, time and camera unit.

Characterisation of Systematic Errors. By relaxing the a priori standard deviations of image observations in the bundle adjustment these systematic errors, together with the effects of other error sources, are projected into image space and can be seen as image residuals. Weighted (inverse of distance) moving average image residuals in both the along- and across-track directions were computed from all the block images, which are shown in Fig. 7. The image residuals were taken from the AT 4 adjustment (see Table III) using highly weighted GPS observations ($\sigma = 2{\cdot}5$ cm) and low weighted image observations ($\sigma = 6$ μm) without self-calibration.

In Fig. 7 three effects can be observed:

(1) A low frequency pattern within each image quarter that might be related to camera head calibration issues (Fig. 8).
(2) A high frequency pattern which might be related to manufacturing CCD accuracy issues or other error sources (Fig. 9).
(3) A "salt-and-pepper" pattern which may come from image matching blunders (Fig. 10).

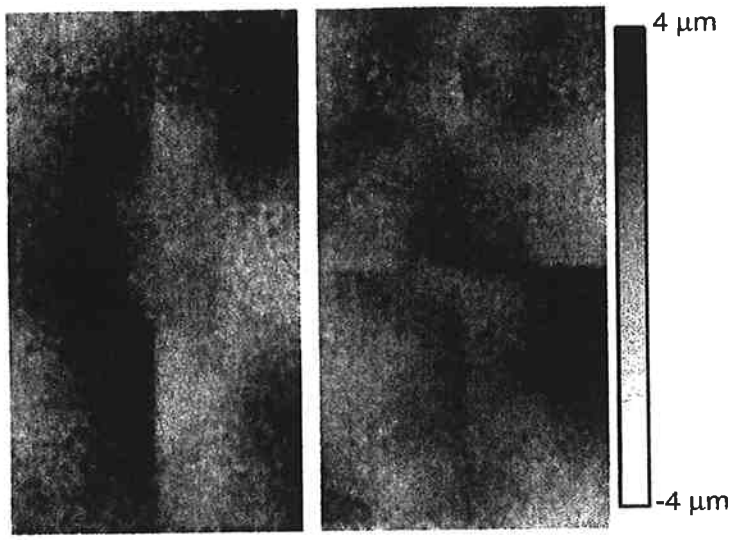

FIG. 7. Weighted (inverse of distance) moving average image residuals, left and right images along- and across-track, respectively (flight direction rightwards).

The range of the residual values shown is approximately −3 to 3 µm in all four image quarters (see Fig. 7), which corresponds to half the pixel size.

Fig. 8 was derived by minimum least squares approximation using a bivariate polynomial of degree seven in each image quarter for the residuals shown in Fig. 7. The polynomial approach serves to characterise only the low frequency systematic errors and is not considered to be a proposal for additional parameters in bundle block adjustment. Further work should find an adequate functional model that can better describe these low frequency systematic errors.

Fig. 9 plots the remaining residuals shown in Fig. 7 once low frequency systematic errors (Fig. 8) have been subtracted.

Stability of Systematic Errors in Image Space. In this subsection low frequency systematic errors in the image space are investigated. The analysis was conducted on four data-sets: 330, 362, 470 and Castell. Blocks 330, 362 and 470 were flown at 4500 m altitude (GSD of 45 cm),

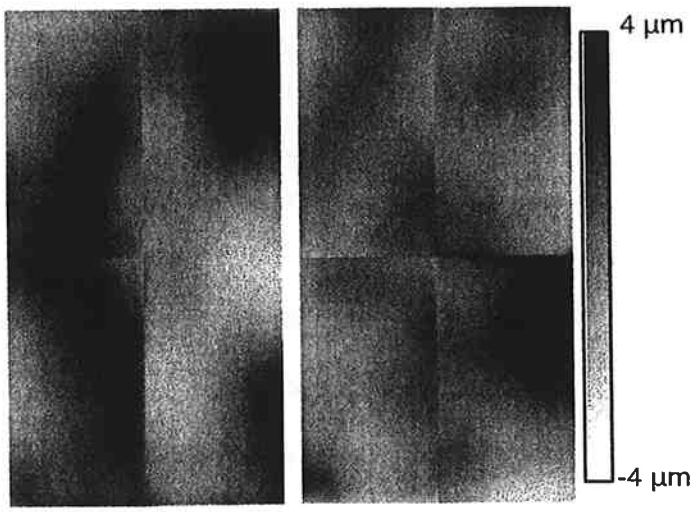

FIG. 8. Low frequency systematic errors derived from Fig. 7, left and right images along- and across-track, respectively (flight direction rightwards).

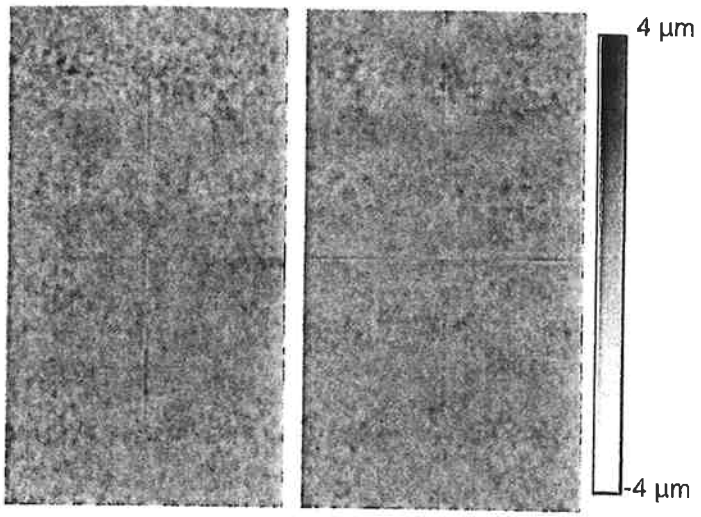

FIG. 9. High frequency systematic error derived by subtracting Fig. 8 from Fig. 7, left and right images along- and across-track, respectively (flight direction rightwards).

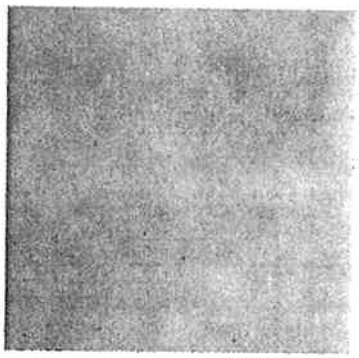

FIG. 10. Detail from along-track residuals in Fig. 7, high frequency and "pepper-and-salt" errors are visible.

with 330 and 362 on the same day and 470 three weeks later. Block Castell was flown at 750 m altitude (GSD of 7·5 cm), three weeks earlier than blocks 330 and 362.

As with the Rubí data-set, bundle block adjustments were performed (one per block) with low image observation weighting and high GPS observation weighting. Low frequency systematic errors were then computed for each block. In Fig. 11 the along- and across-track low frequency systematic errors are plotted as vectors at each node of a 27×49 grid. It becomes clear that each image quarter shows a different non-symmetric pattern reflecting the four-camera-head geometry of the DMC, and the plots of the four different blocks are similar but not identical.

In Fig. 12 the systematic errors of block 330 are subtracted from the systematic errors of the other blocks. Thus, it becomes more evident that the four blocks show similar trends (see Fig. 12). Two interesting observations can be made: (a) for the same flying altitude (blocks 330, 362 and 470) the difference in low frequency systematic errors increases with time and (b) larger differences are detected in block Castell, which was flown at a different altitude. Current data suggests that stability of systematic errors in image space is more sensitive to flying altitude variations than to time variations.

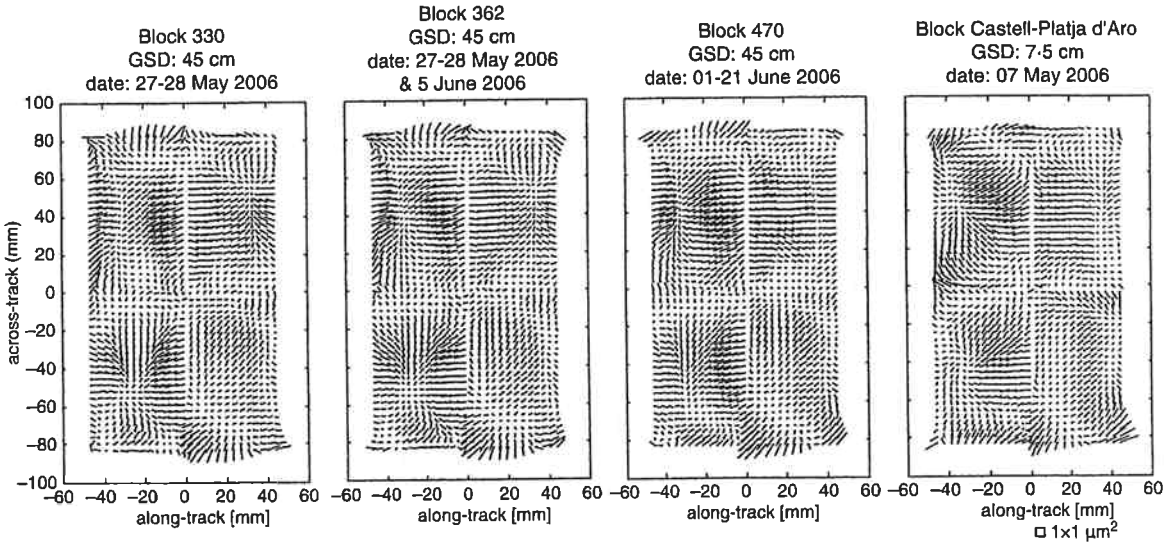

FIG. 11. Low frequency systematic errors in image space computed in blocks 330, 362, 470 and Castell.

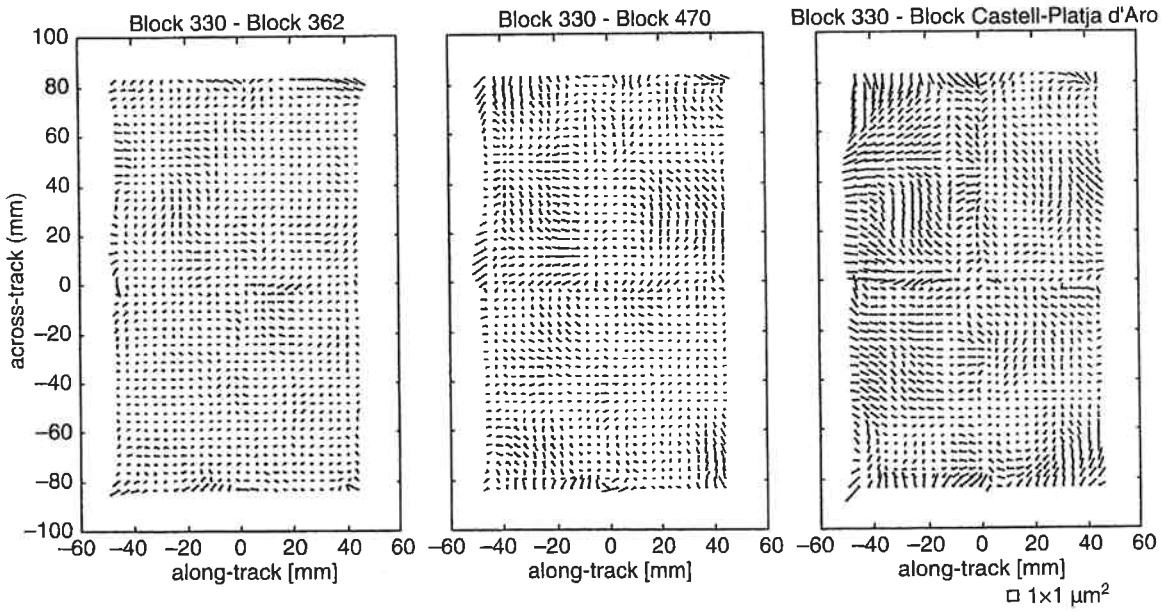

FIG. 12. Differences in low frequency systematic errors in image space of blocks 362, 470 and Castell taking block 330 as a reference.

Prior to this work, stability was investigated in four data-sets, two of them flown at an altitude of 4500 m and the other two flown at an altitude of 1000 m approximately (Riesinger, 2007). It is shown that the mean image residuals of each block can be reduced to 60% when the mean image residuals of all blocks are averaged and subtracted from each block. This percentage increases to 80% when only the mean image residuals of the two data-sets with a similar flying height configuration are averaged. Such results suggest that there is a height dependency of systematic errors in images. Nevertheless, as the low- and high-altitude flights

were taken three months apart, the possibility that such errors also depend on time cannot be excluded.

In Fig. 13 the low frequency systematic error patterns computed in block Rubí (flown with camera DMC01-0014) and in block 330 (flown with camera DMC01-0026) are plotted. This shows that each DMC camera has its own different systematic error pattern.

Modelling Systematic Errors in Image Space

This section is dedicated to discussing how these systematic errors can be modelled or calibrated. Two different approaches are considered: (a) the use of self-calibration parameters and (b) the application of correction grids.

Role of Self-calibration Parameters. This subsection discusses the extent to which the four sets of 12 self-calibration parameters (Ebner, 1976) are capable of modelling the low frequency systematic errors in image space described here (see Fig. 8).

Thus, the weighted (inverse of distance) mean image residuals in Fig. 11 were computed in the same way as those in Fig. 7, after four sets of 12 self-calibration parameters had been applied in the bundle adjustment (see Fig. 14). Although the range of low frequency systematic error shown in Figs. 7 and 8 is reduced by 50% from ±3·0 to ±1·5 μm in each image quarter, Fig. 14 still shows some of the low frequency systematic errors that are not modelled by a polynomial approach of degree two (such as the 12 self-calibration parameters). This means that the 4×12 parameter approach improves height accuracy significantly (see above), but it is not the most appropriate set of parameters to handle the low frequency systematic errors shown in Fig. 8. Further work should analyse a suitable set of self-calibration parameters capable of modelling low frequency systematic errors properly.

Removing Systematic Errors in Image Space. Another approach to modelling the systematic errors is the computation of correction grids in the virtual image (see Dörstel, 2007), which is analysed in this subsection. Stability of the correction grids over time is a requirement to fully exploit the potential of this approach as a calibration procedure.

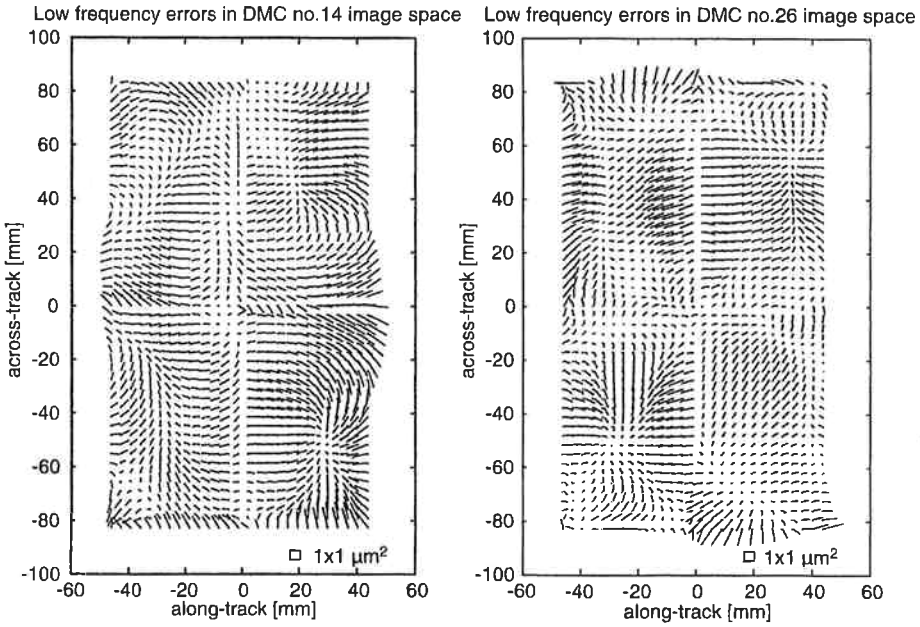

FIG. 13. Low frequency systematic error patterns for DMC01-0014 and DMC01-0026 cameras.

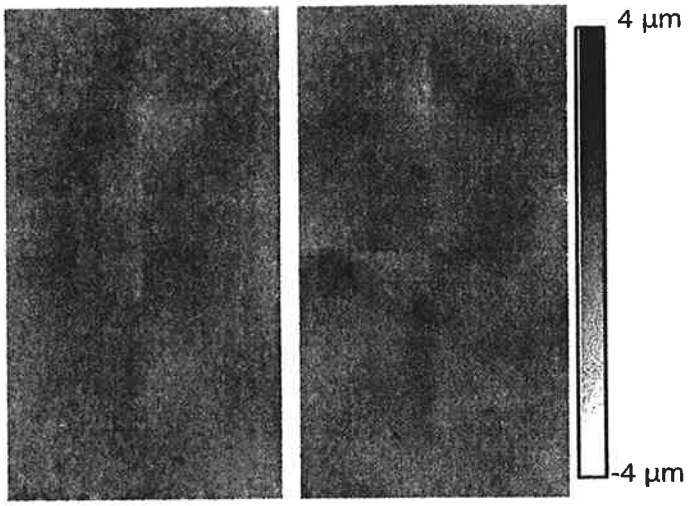

FIG. 14. Weighted (inverse of distance) moving average image residuals when four sets of 12 self-calibration parameters are used, left and right images along- and across-track, respectively (flight direction rightwards).

At the AT 4 in the Rubí data-set a low frequency correction grid was computed from data in Fig. 8 with a 288 µm spacing for each image component (x along-track and y across-track). Then, for any photogrammetric observations, a low frequency correction was computed for each image component by bilinear interpolation of the low frequency correction grid. Finally, the photogrammetric observations were modified by removing the low frequency correction and a new bundle adjustment was performed by using 10 cm a priori GPS accuracy, 2 µm a priori image pointing accuracy and no additional self-calibration parameters. Under these conditions, in AT 4 the rms height accuracy at the 20 check points was reduced from 85·3 to 47·9 cm, which corresponds to a 43% improvement in height.

In order to prove whether systematic errors still remain, the a priori standard deviations of the image observations are relaxed down to 6 µm and the weights of the GPS observations are increased to 2·5 cm, any systematic error source (still unmodelled in the above paragraph) is moved into the image space (as described in earlier sections). Then the weighted (inverse of distance) moving average image residuals in both the along- and across-track directions were computed (see Fig. 15). In Fig. 15 some remaining systematic errors are still visible, which the applied correction grid has not fully modelled. The behaviour of these errors is different in each image quarter, which indicates that this approach is not able to solve the problems derived from DMC geometry completely in a single step.

In a next step the correction grid was iteratively refined using the procedure described above: at iteration i the low frequency correction grids were derived from the residuals in image space at iteration $i - 1$; the image observations (at iteration i) were corrected by removing the low frequency correction (interpolated from the low frequency grids); afterwards, a bundle block adjustment with low weighted image observations, highly weighted GPS observations and no self-calibration parameters was performed, obtaining residuals in image space at iteration i. The evolution of this iteration process is summarised in Table IV, and, despite the slow convergence of the method, it is proved that the expected theoretical accuracy was reached at iteration 16, obtaining 5·4 cm rms in height at check points in the Rubí data-set.

This procedure of course has low practical significance if it must be applied individually to any data-set. Further work should validate the extent to which this kind of characterisation/

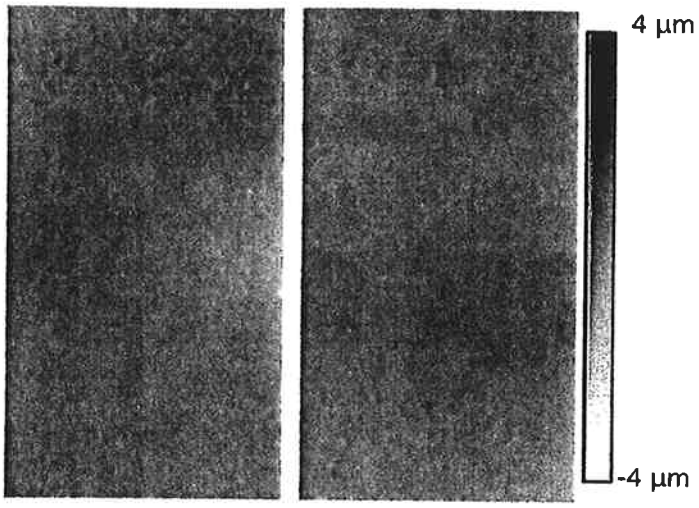

FIG. 15. Weighted (inverse of distance) moving average image residuals when low frequency systematic corrections corresponding to Fig. 8 are applied to the image observations, left and right images along- and across-track, respectively (flight direction rightwards).

TABLE IV. Evolution of the rms errors at the 20 check points of block Rubí in iterations 0 to 16 of AT 4 (iteration 0 corresponds to AT 4 with no systematic error correction at all and iteration i corresponds to image observations used in iteration $i - 1$ and corrected by removing systematic error grids computed in iteration $i - 1$).

Iteration	*0*	*1*	*2*	*3*	*4*	...	*16*
X (m)	0·057	0·042	0·037	0·035	0·033	...	0·029
Y (m)	0·068	0·055	0·050	0·046	0·044	...	0·039
H (m)	0·853	0·479	0·311	0·225	0·175	...	0·054

calibration procedure is able to compensate for systematic errors to other data-sets, as discussed in Dörstel (2007) and Madani and Shkolnikov (2008).

CONCLUSIONS

A theoretical accuracy analysis has shown that the B/H ratio handicap of the DMC is compensated by higher image pointing accuracy in conjunction with accurate GPS observations and a high number of tie point measurements generated by image matching techniques. Theoretically it is possible to achieve comparable height accuracies with block set-ups of analogue cameras under the following conditions: image pointing accuracy between 1·2 and 1·5 µm, GPS observations with 10 cm accuracy (σ) and a dense pass/tie point distribution.

As doubling the image pointing accuracy does not compensate in bundle adjustment for the reduction by a factor of 2 of the B/H ratio, higher accuracy in control and/or GPS data or a very dense tie point distribution is required to handle and keep under control the error propagation through the block. It should be noted that this conclusion is derived from theory and synthetic data-sets only. Similar conclusions could be drawn for any other camera with a B/H ratio lower than 0·6.

In practice for some DMC data-sets unexpectedly large height errors are obtained, especially if the blocks are highly connected (with a large number of image observations and corresponding object (pass/tie) points) and if only poor or even no GPS data observations are available. Nevertheless, self-calibration with four independent sets of 12 parameters (one for

each image quadrant) in the block adjustment yields significant improvement in the results. This approach is able to model systematic errors well enough to reach the theoretical accuracies and precisions predicted in published papers about the DMC. However, it is not able to model all low frequency systematic errors in image space. This requires a higher order polynomial approach (or a more appropriate functional model) than the second order used in the 12 parameter model.

Two different types of systematic errors in image space are detected: low frequency systematic errors, which can be partially modelled by the four sets of 12 additional parameters, and high frequency systematic errors. The former could be related to camera head calibration issues while the latter could be caused by CCD chip manufacturing precision. Different DMC cameras have different systematic error patterns in image space.

An iterative method to characterise/calibrate low frequency systematic errors in image space as correction grids is presented. This method is proved to fully model, in the calibration data-set, those systematic errors in image space to reach the theoretical accuracies and precisions expected for the DMC. Further work should validate this method as a calibration process capable of application to other data-sets.

Stability analysis of low frequency systematic errors in image space suggests that there could be a height or time dependency. It is critical to prove whether systematic errors in image space are stable in relation to time and flying height, which is a precondition for applying their characterisation and calibration in the virtual image generation process. If further work demonstrates the instability of systematic errors in image space, a suitable and rigorous set of additional self-calibration parameters will be required.

REFERENCES

ALAMÚS, R., KORNUS, K., PALÀ, V., PÉREZ, F., ARBIOL, R., BONET, R., COSTA, J., HERNÁNDEZ, J., MARIMON, J., ORTIZ, M. A., PALMA, E., PLA, M., RACERO, S. and TALAYA, J., 2005. Validation process of the ICC digital camera. *ISPRS Hannover Workshop 2005 on High-Resolution Earth Imaging for Geospatial Information*. 6 pages (on CD-ROM).

ALAMÚS, R., KORNUS, W. and TALAYA, J., 2006. Studies on DMC geometry. *ISPRS Journal of Photogrammetry and Remote Sensing*, 60(6): 375–386.

CRAMER, M., 2007. *DMC User Forum*. http://www.ifp.uni-stuttgart.de/eurosdr/Gaevle07-EuroSDR-DMC.pdf [Accessed: 1st March 2007].

DÖRSTEL, C., 2003. DMC—practical experiences and photogrammetric system performance. *Photogrammetric Week 2003* (Ed. D. Fritsch). 292 pages: 59–65.

DÖRSTEL, C., 2007. DMC—(r)evolution on geometric accuracy. *Photogrammetric Week 2007* (Ed. D. Fritsch). 350 pages: 81–88.

DÖRSTEL, C., JACOBSEN, K. and STALLMANN, D., 2003. DMC—photogrammetric accuracy—calibration aspects and generation of synthetic DMC images. *Optical 3-D Measurement Techniques VI* (1) (Eds. A. Grün & H. Kahmen). 388 pages: 74–82 (also on CD-ROM). http://www.ipi.uni-hannover.de/uploads/tx_tkpublikationen/Jac0903zuerich.pdf [Accessed: 4th September 2008].

EBNER, H., 1976. Self calibrating block adjustment. *Bildmessung und Luftbildwesen*, 44(4): 128–139.

HEFELE, J. and DÖRSTEL, C., 2007. *Mid exposure pulse versus start exposure pulse*. Unpublished communication to the DMC User Network in digital form.

HINZ, A., 1999. The Z/I Digital Aerial Camera system. *Photogrammetric Week 1999* (Eds. D. Fritsch & R. H. Spiller). 380 pages: 109–115.

HONKAVAARA, E., AHOKAS, E., HYYPPÄ, J., JAAKKOLA, J., KAARTINEN, H., KUITTINEN, R., MARKELIN, L. and NURMINEN, K. 2006a. Geometric test field calibration of digital photogrammetric sensors. *ISPRS Journal of Photogrammetry and Remote Sensing*, 60(6): 387–399.

HONKAVAARA, E., JAAKKOLA, J., MARKELIN, L., NURMINEN, K. and AHOKAS, E. 2006b. Theoretical and empirical evaluation of geometric performance of multi-head large format photogrammetric sensors. *International Archives of Photogrammetry, Remote Sensing and Spatial Information Sciences*, 36(1): 56–61. Also 6 pages (on CD-ROM).

MADANI, M. and SHKOLNIKOV, I., 2008. Further investigation into geometric accuracy of DMC. *International Calibration and Orientation Workshop EuroCOW 2008*. 13 pages (on CD-ROM).

RIESINGER, I., 2007. *Investigations on DMC (digital metric camera) auto-calibration*. Unpublished diploma thesis, Technische Universität München. 92 pages.

SCHROTH, R. W., 2007. Large format digital cameras for aerial survey of geospatial information. *FIG Working Week 2007*. 15 pages (on CD-ROM).

ZEITLER, W., DÖRSTEL, C. and JACOBSEN, K. 2002. Geometric calibration of the DMC: method and results. *International Archives of Photogrammetry and Remote Sensing*, 34(1): 324–333. Also 6 pages (on CD-ROM).

Résumé

Depuis l'apparition des premières caméras aériennes numériques à grand format, leurs performances font l'objet de grandes attentes. On se rapproche d'images aériennes idéales, virtuellement sans erreurs géométriques et avec une plus grande qualité radiométrique. Cependant, depuis 2005 ont été constatés des résidus-image systématiques, des erreurs altimétriques inattendues lors de l'aérotriangulation et la nécessité de paramètres d'auto-étalonnage supplémentaires. Dans cet article, à la lumière de ces publications récentes, une analyse préliminaire des précisions théoriques de l'aérotriangulation des caméras numériques DMC de Zeiss/Intergraph (Z/I) et analogiques est menée. Cette analyse considère un modèle mathématique où l'image a une géométrie conique et où les erreurs systématiques sont absentes. L'influence sur la précision résultante dans le bloc, du rapport base sur hauteur, de la précision de pointé dans les images (manuel et automatique), des observations GPS pour les centres de projection ainsi que la densité de points de liaison est étudiée. De plus, la précision attendue pour l'aérotriangulation des images analogiques en utilisant le processus actuel d'aérotriangulation (la précision a priori du pointé dans les images, de la mesure des points d'appui et de la densité des points GPS et de liaison) est calculée. Le but de cette étude théorique est de trouver des critères pour l'aérotriangulation avec les données DMC qui devraient donner le même sinon un meilleur degré de précision que celui obtenu avec les données analogiques dans les mêmes conditions.

Dans la partie suivante, les conclusions de cette analyse théorique sont vérifiées à partir de jeux de données réels et du processus d'aérotriangulation et s'accordent avec l'analyse théorique. Les résultats montrent que la précision théorique attendue pour l'aérotriangulation n'est obtenue que si l'on introduit un jeu de paramètres d'auto-étalonnage approprié pour l'ajustement de faisceaux par bloc et/ou si de bonnes observations GPS sont disponibles. La propagation défavorable venant d'erreurs systématiques non modélisées dans les blocs d'images DMC entraîne de telles conditions pour l'aérotriangulation. Plusieurs auteurs ont constaté des résidus systématiques de l'ordre du dixième de pixel (en emq) dans l'espace-image DMC. Pour cette raison, des investigations sont menées sur la caractérisation des erreurs systématiques, leur distribution dans l'espace-image, leur stabilité en fonction du temps et de la hauteur de vol et leur modélisation en utilisant des jeux de paramètres auto-étalonnage et en appliquant des grilles de correction. Finalement, on a pu établir des conclusions à l'issue des recherches menées.

Zusammenfassung

Seit dem Erscheinen der ersten grossformatigen digitalen Luftbildkameras werden hohe Erwartungen an ihre Leistungsfähigkeit gestellt. Der Traum von

Luftbildern, die praktisch frei von geometrischen Fehlern sind und eine verbesserte radiometrische Qualität aufweisen, ist näher gerückt. Gleichwohl wird seit 2005 von systematischen Bildresiduen, unerwarteten Höhenfehlern in der Aerotriangulation (AT) und der Notwendigkeit von zusätzlichen Selbstkalibrierungsparametern berichtet. Motiviert durch die o.g. Veröffentlichungen wird in diesem Beitrag zunächst eine vorbereitende Analyse der theoretischen Genauigkeiten in der AT mit der Digital Mapping Camera (DMC) von Zeiss/Intergraph (Z/I) und einer analogen Luftbildkamera durchgeführt. Sie basiert auf einem mathematischen Modell, das frei von systematischen Fehlern ist und Bilder mit konischer Geometrie voraussetzt. Dabei wird der Einfluss des Basis-Höhen-Verhältnisses, der Bildmessgenauigkeit (sowohl manuell als auch automatisch), der GPS Beobachtungen der Aufnahmezentren und der Verknüpfungspunktdichte auf die Fehlerfortpflanzung und die Genauigkeit des Blocks untersucht. Ferner wird die zu erwartende Blockgenauigkeit mit analogen Luftbildern unter Verwendung aktueller AT-Konfigurationen (a priori Genauigkeit der Bildmessung, der Passpunkte, der GPS-Beobachtungen und Verknüpfungspunktdichte) berechnet. Ziel dieser theoretischen Untersuchung ist es Vorraussetzungen und Bedingungen der AT mit DMC Aufnahmen zu ermitteln, die zu den gleichen oder gar besseren Genauigkeiten führen, als sie mit analogen Aufnahmen unter den gleichen Konditionen erzielt worden wären.

Im darauffolgenden Teil werden die Erkenntnisse aus der theoretischen Untersuchung mit Hilfe von praktischen Daten und AT, die mit den gleichen Parametern gerechnet wurden, überprüft. Die Ergebnisse zeigen, dass die erwartete theoretische Genauigkeit in der AT nur erreicht wird, wenn ein geeigneter Satz von Selbstkalibrierungsparametern verwendet wird und/oder gute GPS Beobachtungen zur Verfügung stehen. Diese Anforderung ist eine Folge ungünstiger Fehlerfortpflanzung von nicht modellierten systematischen Fehlern in DMC Blöcken. Einige Autoren entdeckten bereits sytematische Bildresiduen in der Grössenordnung von 0,1 pixel RMS. Aus diesem Grund wurden die folgenden Untersuchungen durchgeführt. Sie beinhalten die Charakterisierung der systematischen Fehler, die Untersuchung ihrer Verteilung im Bildraum und ihrer zeitlichen Stabilität bei unterschiedlichen Flughöhen und die Modellierung der systematischen Fehler mit Hilfe von Selbstkalibrierungsparameter und Korrekturgittern. Abschliessend werden Schlussfolgerungen aus den Ergebnissen der Untersuchung gezogen.

Resumen

Desde la aparición de las primeras cámaras aéreas digitales de gran formato, se han depositado grandes expectaciones en su rendimiento. El sueño de obtener imágenes aéreas virtualmente libres de errores geométricos y con una calidad radiométrica mayor es más cercano. Sin embargo, residuos sistemáticos en la imagen, inesperados errores en altura en aerotriangulación y la necesidad de parámetros adicionales de auto-calibración han sido reportados desde 2005. En este artículo se lleva a cabo un análisis preliminar de las precisiones teóricas en aerotriangulación de la Digital Mapping Camera (DMC) de Zeiss/Intergraph (Z/I) y una cámara analógica, motivado por las publicaciones mencionadas. En este análisis se considera un modelo matemático donde la imagen tiene una geometría cónica y está libre de errores sistemáticos. Se estudia la influencia en la propagación de la precisión en el bloque de la relación base-altura (B/H del inglés base-to-height ratio), la precisión de medida en la imagen (manual y automática), las observaciones

GPS de los centros de proyección y la densidad de puntos homólogos. Además, se calcula la precisión esperada en aerotriangulación de imágenes analógicas usando las configuraciones "actuales" de aerotriangulación (precisión a priori de las medidas en la imagen, de las medidas de los puntos de control y GPS y la densidad de puntos homólogos). El objetivo de este estudio teórico es dar con los requerimientos para aerotriangular datos DMC con los que se alcance el mismo nivel de precisión, o superior, que los obtenidos con datos analógicos en las mismas condiciones.

En la siguiente parte del artículo las conclusiones de este análisis teórico son comprobadas usando conjuntos de datos reales y configuraciones de aerotriangulación que se corresponden con las del estudio teórico. Los resultados demuestran que la precisión teórica esperada en aerotriangulación es solamente obtenida si se considera en el ajuste del bloque un conjunto de parámetros de autocalibración apropiado y/o si se dispone de buenas observaciones GPS. La necesidad de estos requisitos en aerotriangulación viene dada por la desfavorable propagación de errores sistemáticos no modelados en los bloques de imágenes DMC. Algunos autores han detectado residuos sistemáticos en el espacio imagen de la DMC del orden de un décimo de píxel en error medio cuadrático (rms del inglés root mean square). Por este motivo se llevan a cabo investigaciones en la caracterización de los errores sistemáticos, su distribución en el espacio imagen y su estabilidades el tiempo y la altura de vuelo, y modelado de errores sistemáticos, usando conjuntos de parámetros de auto-calibración y aplicando mallas de corrección en el espacio imagen. Finalmente, las conclusiones son derivadas de las investigaciones.